Zakynthos 25/10/2018, Mw 6.8 earthquake: Superposition of strike-slip and thrust ?

J. Zahradník [1], E. Sokos [2], V. Plicka [1]

[1] Charles University, Prague, Czech Republic
[2] University of Patras, Greece

Report sent to EMSC on 09/11/2018

Introduction On October 10, 22:54 UTC, a significant earthquake (Mw 6.8 GCMT) occurred SW of Zakynthos Island. A thrust-fault foreshock (Mw 4.8 NOA) preceded the event by 32 minutes. Moment tensors of mainshock, reported to EMSC by several agencies, featured a significant variability and large non-DC components. We study possible source complexity with the goal to provide an explanation of the apparently non-shear fault motion. In particular, we investigate possible superposition of mainshock from dominant strike-slip rupture with thrust-faulting, as both can co-exist in regional stress field, and may provide a piece of information about complex tectonic structure of the region.

Epicenter Using the earliest possible manual P-wave picks from broad-band (BB) stations in Greece and a few stations in Italy, together with local strong-motion (SM) stations we relocated mainshock by NonLinLoc probabilistic method [Lomax et al., 2000], see Fig. 1. Epicenter at Lat(°) 37.30, Lon(°) 20.29, and OT 22:54:47 (with the associated probability density function, elongated SW-NE) has been obtained at about 5 km south and 20 km west of NOA epicenter (Lat 37.34, Lon 20.51).

Centroid Deviatoric centroid moment tensor, and all source models in this report, were calculated by ISOLA [Sokos and Zahradník 2008; Zahradník and Sokos, 2018]. Using BB stations at distances 270-630 km, and a low-frequency range of 0.01-0.02 Hz, we obtained centroid position (coinciding by chance with epicenter of AUTH) at 37.39, 20.63, with strike/dip/rake(°) angles of 12/41/165, scalar moment Mo=1.7e19 Nm, DC% ~40, CLVD% ~ -60. The large negative CLVD agrees with NOA solution and is similar to the GCMT solution. Analogous s/d/r angles and low DC% was obtained by using only local SM stations in the frequency range of 0.02-0.05 Hz. Hereafter, the strike/dip/rake(°) angles are abbreviated as s/d/r and shown without the degree sign (°). Centroid position is analogously uncertain in SW-NE direction as epicenter.

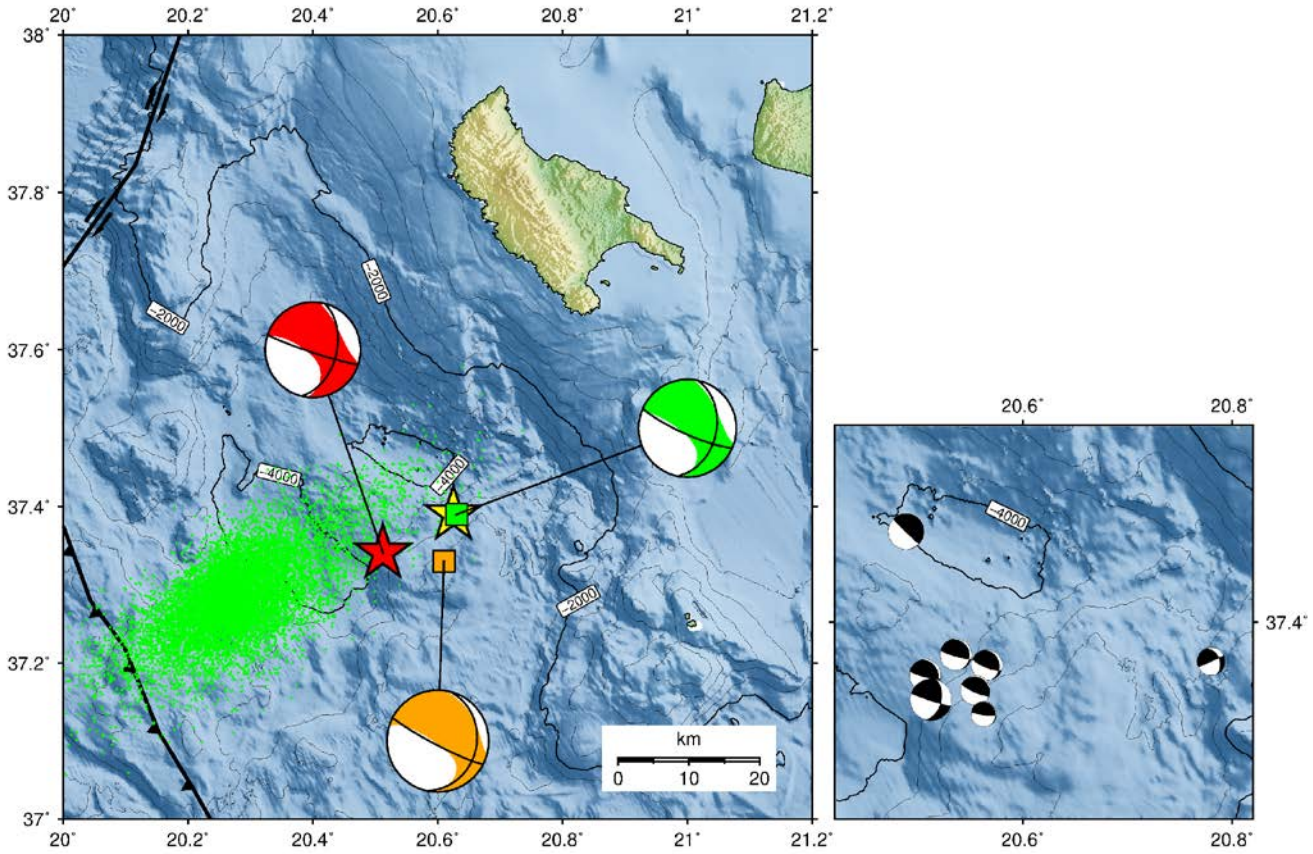

Fig. 1. Epicenter location of this report (green dots), epicenter of NOA (red star), and AUTH (yelow star). Centroid position and deviatoric focal mechanisms of this paper (green square and beachball), that of GCMT (orange), and NOA (red). The local thrust contact of the accretionary wedge of the Mediterranean Ridge, over the Hellenic forearc backstop ('teeth' line), the Kefalonia Transform Fault (black line with arrows) and bathymetry, are also shown. In the small right-hand panel, double-couple focal mechanisms of foreshock and aftershocks, calculated by NOA, are presented. The bathymetry data were obtained from the Hellenic Centre for Marine Research.

Major subevent For major subevent (hereafter abbreviated as sub1), i.e. a dominant moment release point-source, we inverted local SM stations of western Greece in a broader frequency range of 0.02-0.10 Hz, obtaining a typical variance reduction of VR ~ 0.6, see Fig. 2. Horizontal grid search was performed at trial depths of 15, 20, 25, 30 and 35 km, seeking a DC-constrained (i.e. a DC% 100) moment tensor, see Fig. 3. With increasing depth, which can hardly be precisely resolved, sub1 moves closer to the NOA epicenter, and Mo increases, indicating that the 35-km depth would be already too large (Mw > 6.8); the source angles are stable s/d/r ~ 20/40/-170.

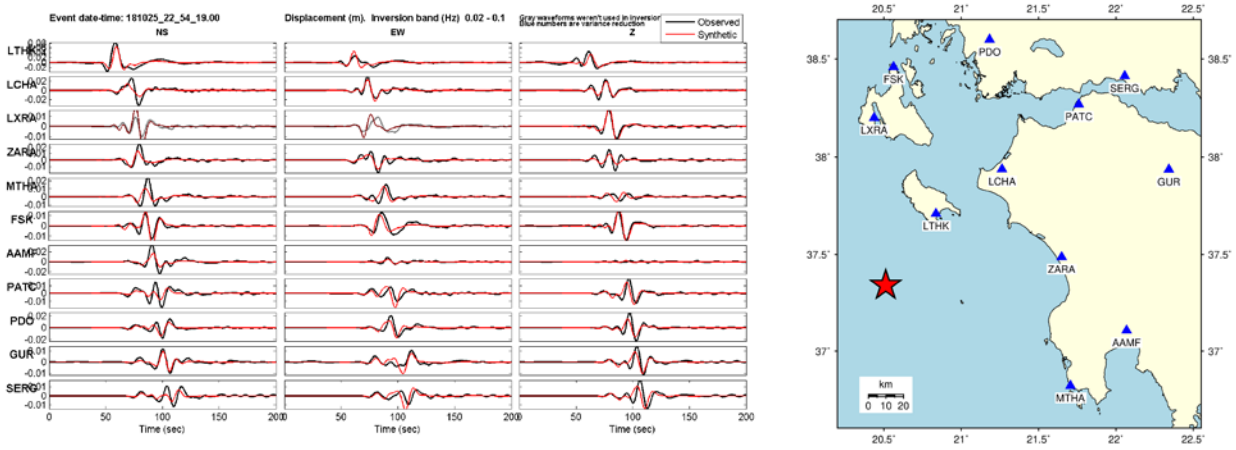

Fig. 2. Waveform match (displacement 0.02-0.10 Hz) of the best-fit solution at depth of 25 km. Simple model of a single-point source, i.e. major subevent, is used. Map of used SM stations: LXRA, LCHA, PATC, ZARA and MTHA belong to NOA strong motion network, whereas LTHK, FSK, PDO, SERG, AAMF, and GUR are operated by the University of Patras and the Charles University.

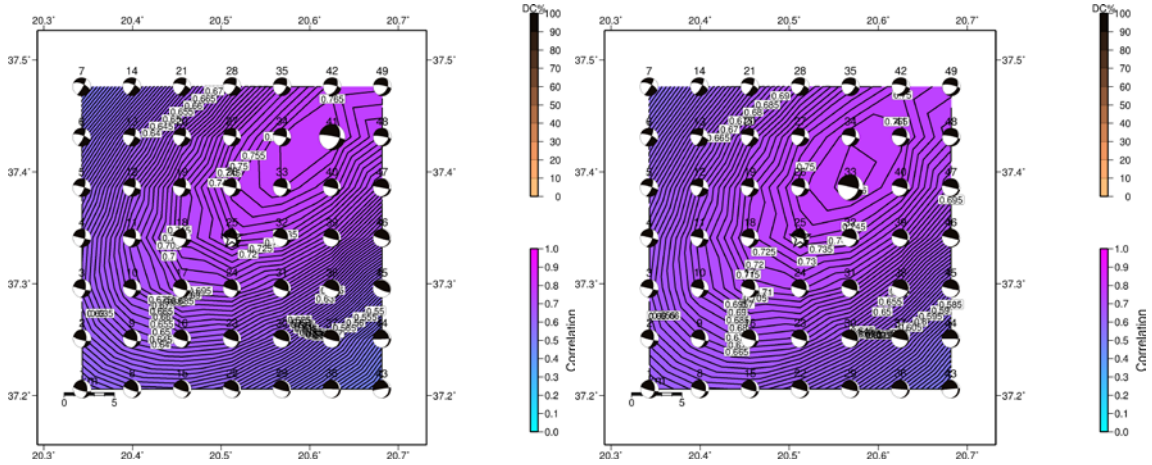

Fig. 3. Horizontal grid search for a DC-constrained major subevent at the depths of 15 km (left) and 25 km (right). The NOA epicenter is shown by star in the middle of the panels. Correlation between real and synthetic waveforms is shown by background color and isolines. The SW-NE elongation of the isolines illustrates uncertainty caused by azimuthal gap of the local strong-motion stations towards SW.

The results show that centroid position and position of major subevent (sub1) can hardly be distinguished from each other. It indicates that fault rupture was spatially and temporally compact. This observation seems to be supported by global back-projections [IRIS]. On the other hand, the non-DC component calls for explanation, most naturally as caused by complexity of the source. Many attempts were made to detect some smaller subevents (sub2, 3, etc.) by means of iterative deconvolution. All tests provided either additional subevents that were too small in terms of moments, sub2 << sub1, or sometimes comparable, e.g. sub2 ~ sub1/3, but both having focal mechanisms of similar type as sub1; this result also points to spatial and temporal proximity of possible subevents, if they exist.

Time function The source time function is calculated in this report by the non-negative-least-square (NNLS) method [Zahradník and Sokos, 2014], implemented in ISOLA. We used the same

SM stations as above, and frequencies 0.02-0.10 Hz. Because the maximum frequency is 0.1Hz, we effectively superimpose ~10-s triangles. We used various assumed source positions and their DC focal mechanisms, constraining or un-constraining total moment value, all with just small differences in the result. We obtain a stable moment-rate function, basically composed of two dominant terms, mutually shifted in time by ~4-5s, providing the source duration of ~15s. This estimate agrees with the ~17-s duration of [GEOSCOPE]. It is also in agreement with the main phase of the ~20-s duration reported in the USGS finite-fault model, comprising two episodes in their time function.

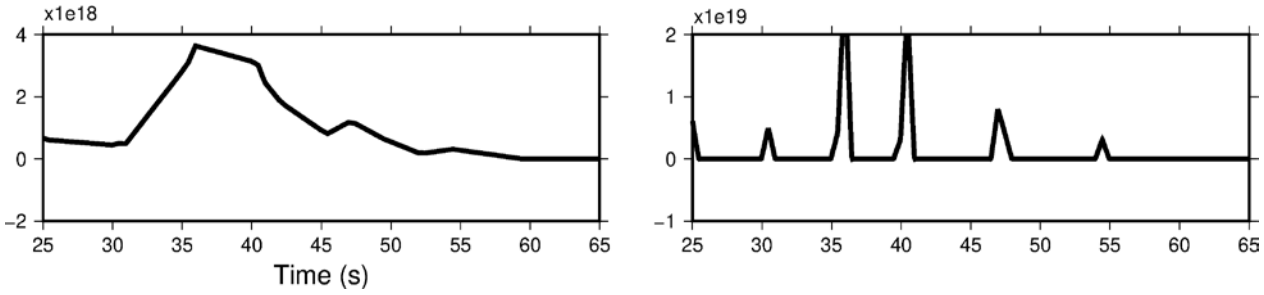

Fig. 4. A typical source-time function obtained in our study. Time 30 s is origin time. Left – moment-rate function superposed from 10-s triangles. Right – the same, but expressed as weighting coefficient of the significant contributions, *formally* shown with 1-s pulses (the inversion up to 0.1 Hz cannot truly resolve 1-s pulses but is sensitive to temporal shift and relative size of the contributions). For this calculation, a single source with the position and focal mechanism of the centroid was used.

Possible thrust-fault (TF) source component In situation described above, when iterative deconvolution cannot resolve position, time and mechanism of smaller subevents (sub2, sub3, …), we suggest a different approach. We start from the non-DC centroid moment tensor (MT), and assume that is composed from just two components. We subtract the 100%DC moment tensor of the above discussed major subevent (MT1), i.e., MT2 = MT - MT1, and we interpret MT2 as a hypothetical subevent 2 whose position and time remains unresolved. In this way we obtain a nearly 100% DC tensor MT2, with s/d/r = **315 /30/ 81** =145 /60/ 95. This result is relatively robust relative to variations in the adopted MT and M1; a more sensible parameter is scalar moment of MT1. Note that all three tensors (Fig. 5) have almost identical direction of the P axis, while T and B tradeoff with each other in the MT1 and MT2 terms.

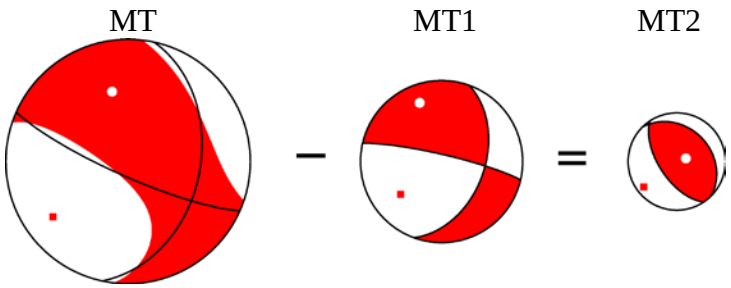

Fig. 5. Subtracting from deviatoric moment tensor of centroid (which significantly deviates from pure DC) the DC tensor of major subevent, we obtain focal mechanisms of hypothetical subevent 2. For short, MT1 is referred to as strike-slip part (SS), and MT2 is pure thrust-faulting mechanism (TF).

Therefore, we have obtained a stable and relatively strong indication that the mainshock source process involved a nearly strike-slip component (SS) in MT1, and a thrust-faulting component (TF) in MT2. Such result is not surprising when considering focal mechanisms of the largest events of the sequence reported to EMSC by NOA (Fig. 1). In fact, there were 6 low-dip (< 20°) thrust faults, all striking at ~300°. Examples: Mw4.8 foreshock (Oct 25, 22:22, s/d/r = 304 /12/ 100) and the first Mw>5 aftershock (Oct 26 05:48, s/d/r = 343 /19/ 147).

Rough estimate of stress field Although the so-far reported focal mechanisms are just few they can be used for the first guess of the stress field (Fig. 6). Using StressInverse code [Vavryčuk, 2014], and excluding two aftershocks M<5, we obtain the following result.

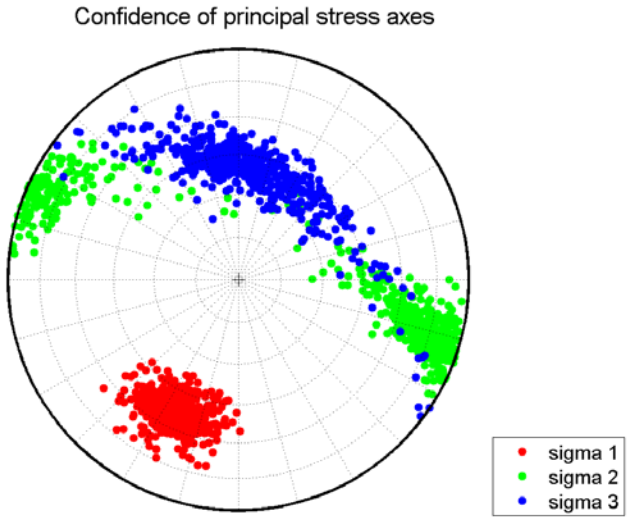

Fig. 6. Preliminary rough estimate of stress field from a few focal mechanisms by StressInverse code. Shown are directions of principal stress axes with their uncertainties.

The principal stress axis Sigma 1, close to P-axes of the analyzed events, is the only well resolved axis. The other two axes tradeoff with each other in the plane perpendicular to Sigma 1, because the corresponding principal stresses (eigenvalues) have similar values. Sigma 1: azimuth 208° (range 200°-230°), plunge 37° (range 30°-50°). Note that the indeterminacy of Sigma2 and 3 explains 'flipping' of the T and B axes of the observed events, exactly as we have seen between MT1 and MT2 in Fig. 5. Similar co-existence of strike-slip and thrust faulting has been found in many regions of the world, including the western Greece earthquake sequence of Cephalonia 2014 [Fig. 7 of Sokos, 2015], although the tectonic regime of the region studied in the present report is different (subduction near Zakynthos versus Kefalonia transform fault).

Thrust faulting may have various explanations, but southwest of Zakynthos a natural explanation seems to be related to subduction process [Fig. 1 of Sachpazi et al., 2016, and Fig. 1 of Kokinou et al., 2006]. The subducting plate is proven by many geophysical methods, including global tomography (e.g. model UU-P07 of van der Meer). Direct seismicity evidence for the slab is very clear below Peloponnese [Fig. 10 of Suckale et al., 2009], while in the region west of Zakynthos it is supported by trust-faulting earthquakes at depths < ~20 km [Fig. 8 of Kokinou et al., 2006]. Seismic reflector (interface) at the depth of ~15 km [Clement et al., 2000] seems to map the top of subducting plate in the area west and south-west of Zakynthos.

It is a matter of interest to compare our stress estimate to global empirical relations relation between Sigma1 and the slab geometry [Fig. 2 of Hardebeck, 2015]. They found that for depth ~30 km, Sigma 1 plunge is ~20-50°, which is in agreement with our Fig. 6. The same paper predicts the plate boundary to be at angle 40-60° relative to Sigma 1, thus we could expect the slab dip of ~ 10-20° degrees. This is in agreement with [Sachpazi et al., 2016]. Although the slab dip is not necessarily

the same as the dip of focal mechanisms, we remind that several thrust-faulting NOA aftershocks indeed have such a dip.

As per local strike of the slab ~300° in the studied region (Fig. 1) we may observe a fit with Fig. 6, too. Indeed, the two mutually trading Sigma 2 and 3 axes indicate this strike. In other words, in vertical cross-section perpendicular to strike of the slab, we may encounter Sigma 1 axis together with the along-dip oriented Sigma 3 (or Sigma 2, due to their uncertainty). One of the axes Sigma 2 and 3 is then parallel to strike of the slab. In this context, the s/d/r angles 315 /30/ 81 of our hypothetical TF subevent 2 might be plausible.

Additional waveform evidence To further study our hypothesis that mainshock consisted of a strike-slip and thrust component we grid-search a plane of trial sources, striking at 300°, and dipping at 30°, passing through a point below NOA epicenter at depth of 25 km. We invert SM waveforms in the range of 0.03-0.08 Hz. In one test we make inversion with fixed (presumably known) 100%DC mechanism defined by s/d/r = 15 /50/ -175, and, in the other test, we use s/d/r = 315 /30 /80. In this way, we search independently for possible position, size and time of a SS and TF event, respectively. We try to see how these two mechanisms, independently of each other, could explain complete data.

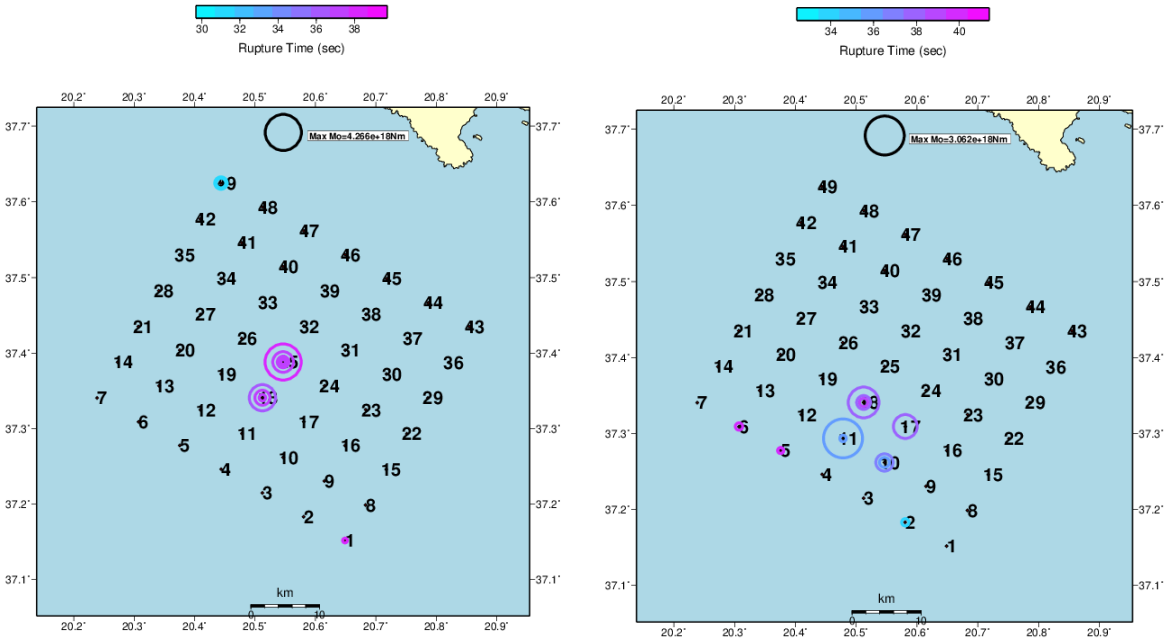

Fig. 7. Independent attempts to explain full waveform data by either SS event (left), or TF event (right). A modified iterative deconvolution with so-called slow moment release is used, to prevent from concentration of moment in sub1. Each circle is a small piece of the moment release which sum-up together.

The results in Fig. 7 and Fig. 8 show that data provide the following model constraints: 1) a SS major subevent at points 25 or 18, time 37s, VR~0.6 or, 2) a TF event at point 11 or 18, time 37s, VR~0.4. We recall that time 30s is origin time. These preferred positions and times in models 1) and 2) are almost the same. This is a proof why iterative deconvolution method cannot separate them into two subevents.

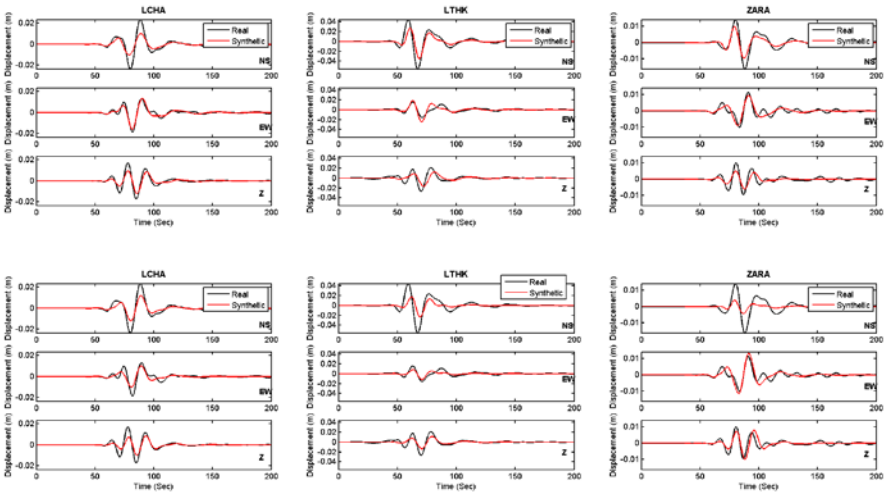

Fig. 8. The waveform fits (displacement 0.02-0.10 Hz) at selected SM stations for the models 1) and 2) discussed above. Top panels – the SS source. Bottom panels – the TF source. Naturally, the fit is better for SS, because SS component dominates in mainshock. Nevertheless, note similarity between the two different data explanations, emphasizing spatial and temporal proximity of SS and TF, shown in Fig. 7.

Joint NNLS inversion of source pairs Being interested in possible TF subevent, that cannot be retrieved by iterative deconvolution, we apply joint search for source pairs, where the two members of each pair have a prescribed mechanism: SS with s/d/r = 15 /50/ -175, and TF with s/d/r = 315 /30 /80. Total moment of each pair is constrained to 2e19 Nm, but relative moment ratio of the two members is free. Each source member has its arbitrary (possibly complex) moment-rate time function. SM data in the range of 0.03-0.08 Hz are used. The pairs are searched in the same trial plane as shown in Fig. 7. All possible combinations of the points of the grid are tested. The result is demonstrated as ensemble of the source pairs whose waveform fit is 'acceptable', i.e. the pairs whose VR > 0.9 VRopt, where VRopt is the best fit. For method, see [Zahradník and Sokos, 2013].

Fig. 9 clearly shows that SS subevents are most likely below the NOA epicenter, (see point No. 18), or at the nearby point 25 (separation of 7 km). Possible positions of the TF subevent are less clearly determined, but for sure they occur in the southern or SW part of the grid, i.e. at the shallower tested depths. For example, depths of points 18 and 25 are 25 and 28.5 km, respectively. Note that TF subevents are weaker than SS (smaller circles in the right panel than in the left one), but TF may occur almost simultaneously with SS – as shown by colors. One pair is the most interesting: (25,4), i.e. SS in point 25 of the left panel, combined with TF in point 4 of the right panel. In this case, the moment ratio TF/SS is the largest possible in the present grid, being of about 0.7/1.3, so TF is definitely not negligible in this case. Closer look on this pair shows that the main peak of the TF moment rate occurs at ~35 s, followed by the SS peak at ~39 s; again OT is at time 30. It is similar to our observation from the point-source time function in Fig. 4. Here, however, we find more details. The mainshock might have developed like this: A weak and early TF subevent with s/d/r = 315 /30 /80 appeared close to epicenter of this study (point 6), at a relatively shallow depth, perhaps 18 km. It was followed by the major SS subevent, with s/d/r = 15 /50/ -175, situated ~10 km deeper, and delayed by ~4 s. Of course, the TF pair member is less certain than SS, but their moment tensor summation gives the observed low DC% = 40-50.

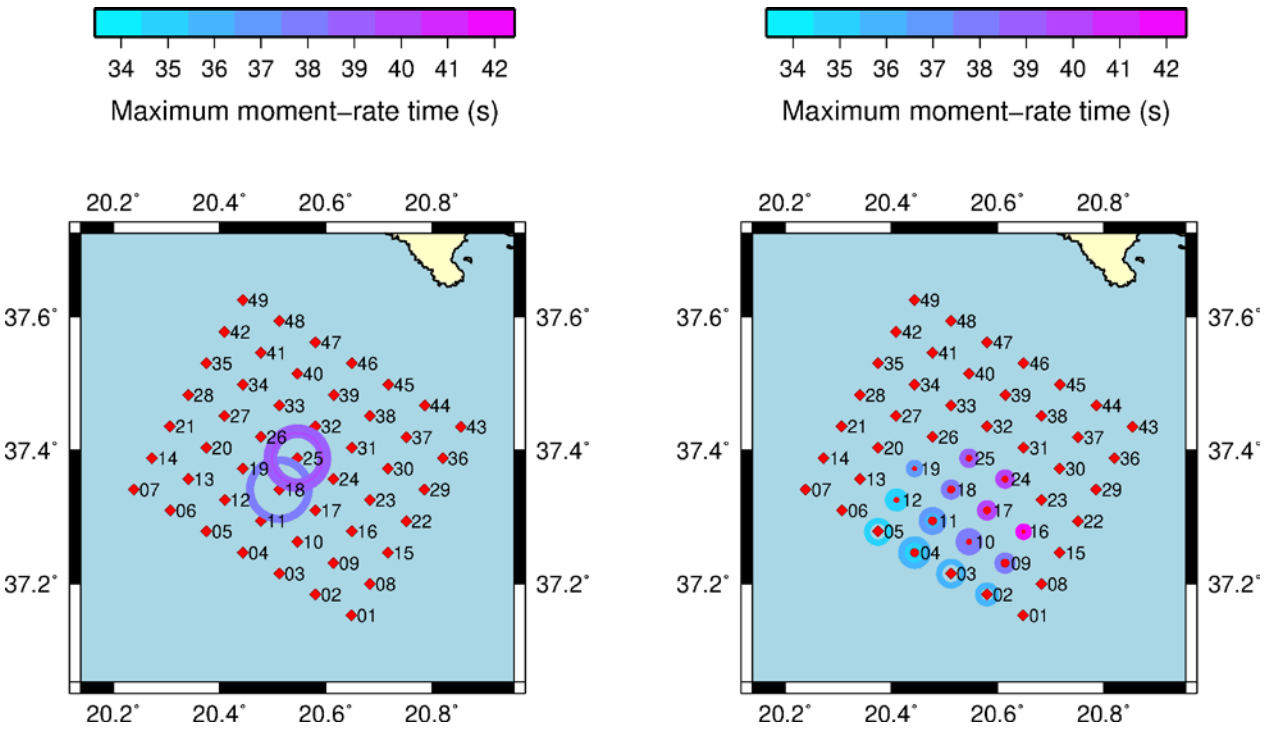

Fig. 9. Joint grid search of source pairs (one member of the pair is strike-slip, SS, and the other is thrust-fault, TF subevent, with prescribed s/d/r angles). The same trial plane as in Fig. 7 is used, striking at 300°, and dipping at 30°. This NNLS method is free from limitations of iterative deconvolution and represents better approach for the spatially and temporary nearby subevents. Left – likely position, size and timing for the SS member of the pairs. Right – the same for the TF member. Time of occurrence of the main peak in moment-rate function is color coded, while the size of the peak scales the circle size. The most interesting pair, discussed in the text, has its early TF subevent at point 4 (depth 18 km), or nearby, and the later dominant SS subevent at point 25 (depth 28 km).

Summary We investigated possible source complexity (two events delayed to each other by ~4 s), indicated by the time function of centroid. Stress regime in the study region allows co-existence of strike slip (SS) and thrust-fault (TF) events due to tradeoff between two principal stresses of similar size, as also supported by aftershocks. We conclude that mainshock might have consisted of two events. First, a weak and early TF subevent with s/d/r = 315 /30 /80 appeared close to epicenter of this study (point 6), at a relatively shallow depth. In our most preferred model of Fig. 9, the TF event likely occurred at the depth of 18 km. Due to uncertainty, we can consider this event situated on the plate boundary (see the above discussed 15-km interface). Then, the weak TF event was followed by a major SS subevent, with s/d/r = 15 /50/ -175, situated ~10 km deeper, and delayed by ~4 s.

Of course, the TF is less well determined than SS, but their moment tensor summation gives the observed low DC% = 40-50. We speculate that either both events occurred on the same weakly-dipping plane, or a deeper (major) SS event occurred on a fault with a somewhat higher dip. The latter might perhaps be related to the non-planar geometry of the plate boundary, or it may imply that the SS event was situated inside the slab. Note that although the rake angles (80 for TF and -175 for SS) are apparently very different, thanks to the accompanying difference in the strike (315 for TF and 15 for SS), both slip vectors point in fact to the similar SW direction.

The proposed mixed TF-SS nature of the mainshock is obviously interesting, but we must emphasize that the analysis suffers from the lack of near stations above the fault and from azimuthal gap toward Ionian Sea. Alternative explanations of the source complexity with a sequence of a very few nearby events of dominantly SS mechanism is possible, but, in contrast to our model, it does not explain the observed non-DC component of mainshock.

Important, but very difficult question, is whether we should keep considering the non-DC mechanism as apparent, or rather investigate the possibility of a truly non-shear faulting.

Further work plan is straightforward: (i) Aftershocks will better delineate fault geometry and improve stress-field estimate. (ii) Finite-fault models should consider possible segmentation of the fault (variable dip and focal mechanism). (iii) Seismic evidence should be combined with geological data about the subducting slab and other faults. (iv) Strong uncertainty due to azimuthal gap should be taken into account. In any case, this event represents a rare possibility to illuminate shallow subduction west of Peloponnese.

Acknowledgment

The seismological data used were derived from the National EIDA node hosted at the National Observatory of Athens (NOA), http://eida.gein.noa.gr/. Data from the Geodynamic Institute of the National Observatory of Athens (doi:10.7914/SN/HL) and the University of Patras (UPAT) (doi:10.7914/SN/HP) were used. The bathymetry data were obtained from the Hellenic Centre for Marine Research. Figures were created using Generic Mapping Tools. V.P., J.Z. and joint Patras-Prague operation of some used stations were partially supported by Czech-Geo/EPOS grant (LM2015079). E. S. acknowledges financial support by the HELPOS Project, "Hellenic Plate Observing System" (MIS 5002697). The authors would like to thank C. Evangelidis for his help and discussions during preparation of this report.

References

Clément, C., A. Hirn, P. Charvis, M. Sachpazi, F. Marnelis (2000). Seismic structure and the active Hellenic subduction in the Ionian islands. Tectonophysics 329 (1-4), 141-156. https://doi.org/10.1016/S0040-1951(00)00193-1

Hardebeck, J. L. (2015). Stress orientations in subduction zones and the strength of subduction megathrust faults. Science 349, 1213 – 1216.

Kokinou, E., E. Papadimitriou, V. Karakostas, E. Kamberis, F. Vallianatos (2006). The Kefalonia Transform Zone (offshore Western Greece) with special emphasis to its prolongation towards the Ionian Abyssal Plain. Mar Geophys Res 27:241–252 DOI 10.1007/s11001-006-9005-2

Lomax, A., J. Virieux, P. Volant, and C. Berge (2000). Probabilistic earthquake location in 3D and layered models: introduction of a Metropolis-Gibbs method and comparison with linear locations, in Advances in Seismic Event Location, C. H. Thurber and N. Rabinowitz (Editors), Kluwer, Amsterdam, 101–134.

Sachpazi, M., M. Laigle, M. Charalampakis, J. Diaz, E. Kissling, A. Gesret, A. Becel, E. Flueh, P. Miles, and A. Hirn (2016). Segmented Hellenic slab rollback driving Aegean deformation and seismicity, Geophys. Res. Lett., 43, 651–658, doi:10.1002/2015GL066818

Sokos, E.N., Zahradník, J. (2008). ISOLA a Fortran code and a Matlab GUI to perform multiple-point source inversion of seismic data. Comput. Geosci. 34, 967–977. doi:10.1016/j.cageo.2007.07.005

Sokos, E., Kiratzi, A., Gallovič, F., Zahradník, J., Serpetsidaki, A., Plicka, V., Janský, J., Kostelecký, J., Tselentis, G.A. (2015). Rupture process of the 2014 Cephalonia, Greece, earthquake doublet (Mw6) as inferred from regional and local seismic data. Tectonophysics 656, 131–141. doi:10.1016/j.tecto.2015.06.013

J. Suckale, S. Rondenay, M. Sachpazi, M. Charalampakis, A. Hosa, L. H. Royden (2009). High-resolution seismic imaging of the western Hellenic subduction zone using teleseismic scattered waves, Geophysical Journal International, 178 (2), 775–791, https://doi.org/10.1111/j.1365-246X.2009.04170.x

van der Meer, D.G., van Hinsbergen, D.J.J., and Spakman, W. (2018). Atlas of the Underworld: slab remnants in the mantle, their sinking history, and a new outlook on lower mantle viscosity, Tectonophysics 723, p. 309-448

Vavryčuk, V. (2014). Iterative joint inversion for stress and fault orientations from focal mechanisms, Geophysical Journal International, 199, 69-77, doi: 10.1093/gji/ggu224

Zahradník, J., and E. Sokos (2018). ISOLA code for multiple-point source modeling—Review, in Moment Tensor Solutions—A Useful Tool for Seismotectonics, S. D'Amico (Editor), Springer Natural Hazards, Cham, Switzerland, doi: 10.1007/978-3-319-77359-9_1

Zahradník, J., Sokos, E. (2013). The Mw 7.1 Van, Eastern Turkey, earthquake 2011: two-point source modelling by iterative deconvolution and non-negative least squares. Geophys. J. Int. 196, 522–538. doi:10.1093/gji/ggt386

Web pages

NOA, http://bbnet.gein.noa.gr/HL/

AUTH, http://geophysics.geo.auth.gr/ss/

EMSC, https://www.emsc-csem.org/ #2w

USGS, https://earthquake.usgs.gov/earthquakes/eventpage/us1000hhb1/executive

IRIS, https://ds.iris.edu/ds/products/backprojection/

GEOSCOPE, http://geoscope.ipgp.fr/index.php/en/data/earthquake-data/latest-earthquakes